IEEE Access
Multidisciplinary | Rapid Review | Open Access Journal

Received June 26, 2019, accepted July 18, 2019, date of publication July 22, 2019, date of current version August 8, 2019.

*Digital Object Identifier 10.1109/ACCESS.2019.2930353*

# Stabilization Control Mothed for Two-Axis Inertially Stabilized Platform Based on Active Disturbance Rejection Control With Noise Reduction Disturbance Observer

**FAN WANG[1,2], RANJUN WANG[1], ENHAI LIU[1], AND WENMING ZHANG[1]**
[1]Institute of Optics and Electronics, Chinese Academy of Sciences, Chengdu 610209, China
[2]University of Chinese Academy of Sciences, Beijing 100149, China

Corresponding author: Ranjun Wang (wrjwzf@163.com)

This work was supported by the National Natural Science Foundation of China under Grant 61501429.

**ABSTRACT** To improve the stability accuracy of two-axis inertially stabilized platform (ISP) for airborne star tracker application, a stable control method based on active disturbance rejection control (ADRC) is presented to handle the system nonlinearities, parameter uncertainties, and disturbances. A noise reduction method based on a modified disturbance observer (DOB) structure is proposed to suppress sensor noise and improve anti-disturbance capability and rapidity. Moreover, the robust stability of the proposed method is discussed. To illustrate the effectiveness of the proposed method, simulations and laboratory experiments are implemented. Finally, the vehicle tracking star experiments are performed. In addition, the contrast results show that for the two-axis ISP the presented controller has superior performance in anti-jamming ability, rapidity, and isolation.

**INDEX TERMS** Inertially stabilized platform, active disturbance rejection control, disturbance observer, robust stability, noise reduction.

## I. INTRODUCTION

Star tracker is widely used in astronomical navigation systems. It is of crucial significance for a star tracker to obtain high-resolution and continuous star images. However, in terms of airborne conditions, due to the attitude change and vibration of the aircraft are more severe than that of the satellite, the line of sight (LOS) of the imaging sensor is difficult to stabilize, which will degrade the star image quality and even cause the target star to be lost.

Inertially stabilized platform (ISP) is the key to solving the stability problem of LOS due to its superior isolation disturbance capability [1], [2]. For airborne ISP, there exist nonideal multisource disturbance including the outer disturbances and the inner disturbances [3]–[5]. Therefore, the ISP system with image payload is a nonlinear time-varying system with parameter perturbation and multi-source disturbance [6]. The vibration isolation function of ISP is realized by measuring carrier disturbance with gyroscope and feeding back to control system. Consequently, ISP needs superior rapidity to respond quickly to gyroscope feedback information. On the other hand, ISP needs strong anti-disturbance capabilities to suppress disturbances, nonlinearities and parameter uncertainties present in the system. Numerous control methods have been developed to improve ISP control performance [3], [7], [8].

Even though advanced control theory has evolved over decades, PID control still dominates in engineering applications, due to fact that advanced control theory requires much model information and is hard to tune and maintain [9]. However, due to the structural limitation of PID controller, it is difficult for PID to deal with parameter uncertainties and nonlinear dynamics. Therefore, its deformations have become very popular in practical applications. For example, some parameter adaptive methods have been studied [10], [11]. Although these parameter adaptive methods can improve the performance of PID, they cannot eliminate the structural defects of the PID so that control performance is still easily deteriorated by disturbance. Robust control can effectively overcome parameter uncertainty and disturbance [12].

The associate editor coordinating the review of this manuscript and approving it for publication was Ming Luo.

  

However, there are at least two reasons why this method is not suitable. First, the implementation of the H∞ controller is complex, and the coefficients of such controllers are generally very fragile [13], and second, this method is generally conservative for the estimation of disturbances and uncertain dynamics. Sliding mode control is frequently reported due to its insensitivity to disturbances and noise [14]. However, when the switching function gain is large the high frequency chattering is difficult to avoid. Neural networks (NN) can handle complex nonlinear problems, so they have been widely concerned in ISP control systems in recent years [15]–[17]. However, on the one hand NN require a lot of data for training. For the ISP system, due to its complicated working environment, the data in actual work is difficult to obtain, and online training is difficult to achieve. On the other hand, the algorithm complexity of NN is generally high, so a lot of computation time is required. Limited by hardware conditions, it is difficult to apply to systems that require extremely high speed such as ISP.

ADRC is a nonlinear control method proposed by Prof. Han [18], [19], which is used to estimate and compensate for uncertainties in the system including model parameter perturbation, nonlinear dynamics, and external disturbances. And linear ADRC was proposed by Gao [20] for the purpose of simplifying parameter tuning and system performance analysis. ADRC consists of three parts: extended state observer (ESO), tracking differentiator (TD), and state error feedback (SEF). ADRC is a controller with good adaptability and robustness, which can effectively improve the dynamic performance of the system [21]. Moreover, this method needs very little model information, and its parameters are easy to tune. Recently ADRC strategy has been applied in ISP control system [22], [23]. And [24] combine ESO and robust control to achieve high-precision tracking control of ISP. In this paper, ADRC will be applied to the stability control of ISP to suppress nonlinear friction, install unbalanced torque, parameter uncertainty and external torque disturbance and to improve the response speed to gyroscope and tracking inputs. However, the large amount of noise present in the speed feedback obtained by encoder differentiation will severely limit the increase of ADRC parameters. Low pass filters (LPF) may be an intuitive choice to attenuate sensor noise. However, as can be seen from Section 3, simply adding LPF may make ADRC lose robustness. Noise reduction disturbance observer (NR-DOB) proposed by [25] can effectively suppress sensor noise and has strong robustness. However, the disturbance attenuation capability of NR-DOB is only related to NR-DOB, but not to the outer loop controller. The combination of NR-DOB and ADRC will offset the superiority of ADRC.

This paper proposes a simplified NR-DOB (SNR-DOB) to reduce the sensor noise while ensuring that the filtered sensor information retains the disturbance information as much as possible. SNR-DOB has a simpler structure and algorithm. Like NR-DOB, the filtering capability of SNR-DOB can be adjusted by choosing the appropriate bandwidth for the LPF. Moreover, the necessary and sufficient conditions for SNR-DOB robust stability are discussed. Compared with NR-DOB, the condition that plant must be the minimum phase system is removed. And the robust stability of SNR-DOB is more dependent on the outer loop controller. To illustrate the superiority of the proposed method, simulations and laboratory experiments are conducted. The results show that SNR-DOB is superior to NR-DOB in terms of anti-disturbance capability or dynamic performance. Finally, to further verify the practical application effect of the proposed control strategy vehicle tracking star experiments are carried out.

The remaining sections of this paper are as follows. Section 2 presents the star tracker ISP and gives its dynamic model. In Section 3, we first introduce the ADRC algorithm, and explain that the simple combination of ADRC and LPF may lead to system loss of robustness. Then the NR-DOB controller is shown and on this basis SNR-DOB controller is presented. The necessary and sufficient conditions for SNR-DOB robust stability are discussed in Section 4. In Section 5, simulations, laboratory experiments and vehicle tracking star experiments are completed to show the superiority of the proposed method. Finally, some concluding remarks are given in Section 6.

## II. DYNAMIC MODEL OF THE ISP SYSTEM

The ISP system is composed of the yaw and the pitch gimbal, as shown in Fig.1. Its length is 0.42 m in, height is 0.3 m, and width is 0.15 m, and its total weight is 8.5 kg. The mirror is used to reflect the starlight for the optical system to receive. The gimbals are directly driven by DC torque motors. The attitude change and vibration of the carrier are measured by the gyroscope which is fixed to the base of the ISP. The rotary electric encoder is used to measure the relative angle

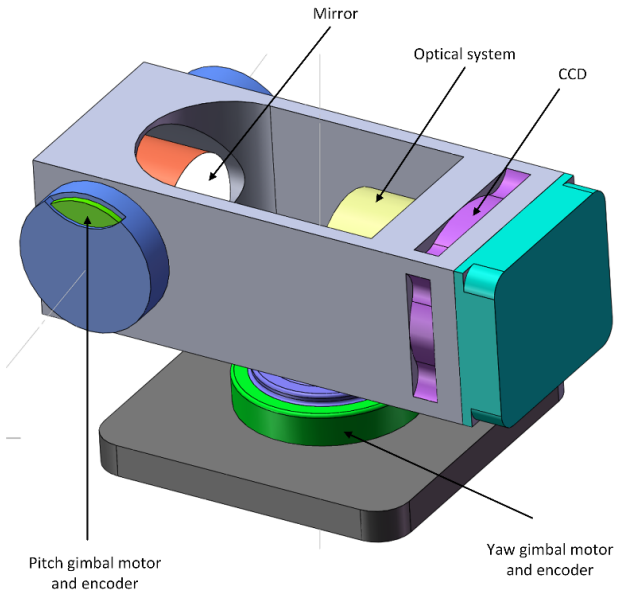


**FIGURE 1.** Schematic diagram of the ISP for airborne star tracker.

of the two gimbals, whose resolution is 24 bits. The sampling frequency of the CCD is 100Hz, and image processing delay time is about 20ms.

ISP compound control systems typically include tracking loop, stabilized loop, and current loop. In order to improve the ISP's dynamic response, disturbance isolation and anti-disturbance capabilities, we are committed to optimizing the stabilized loop in this paper. The stabilized loop with current loop is shown in Fig.2. Current loop is mainly used to improve the dynamic performance of current with voltage. Stabilized loop is the core of ISP system. The ISP's disturbance isolation capability is determined by the Stabilized loop. The rate gyroscope mounted on the carrier is used to detect the motion and vibration of the carrier and feed it back to the stabilized loop in real time to make the motor reverse motion to stabilize the LOS. Photoelectric encoders are used to measure the speed of DC torque motors. The control deviation of the tracking loop is the miss distance, which compensates the distance of the target from the LOS by the tracking loop controller to achieve accurate tracking.

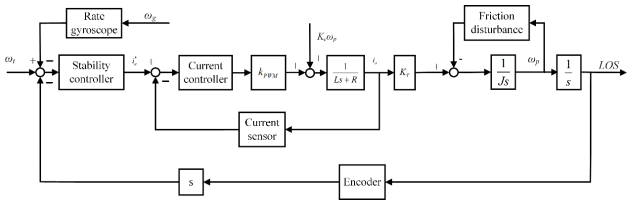


**FIGURE 2.** Stabilization control block of ISP system.

From Fig.2, we know the dynamic model of the ISP mainly depends on the DC torque motor. Detailed derivation of the current loop plant can be found in [26]. $k_{PWM}$ is the PWM coefficient. $J$ indicates the moment of inertia, $R$, $L$, and $K_e$ are the resistance, armature inductance, and motor torque coefficient, respectively. $K_T$ denote the motor torque coefficient. $\omega_t$ is the tracking controller output. $\omega_g$ is the speed at which the carrier's attitude changes, and $\omega_p$ is motor speed. With current closed loop, current loop can be equivalent to an inertia link, then the dynamic model of the DC motor system is simplified to

$$\begin{aligned} \frac{d\omega_p}{dt} &= \frac{K_T}{J} i_a - \frac{1}{J} f_d \omega_p \\ \frac{di_a}{dt} &= -\frac{1}{T_i} i_a + \frac{1}{T_i} i_a^* \end{aligned} \tag{1}$$

where $T_i$ is equivalent inertia time constant, and $f_d$ is equivalent friction coefficient. To accurately describe the dynamic characteristics of the ISP, the Stribeck or LuGre friction model is usually used [24], [27]. According to the friction model, we have $f_d \in [\underline{f}_d, \overline{f}_d]$, where $f_d$, and $\overline{f}_d$ are known positive constants. The transfer function of the stabilized loop plant is

$$P(s) = \frac{K_T}{(T_i s + 1)(Js + f_d)} \tag{2}$$

where $T_i$ is equivalent inertia time constant of the current loop. In fact, due to installation errors, back EMF and different frequency working environments, $J$, $K_T$, and $T_i$ all have certain parameter uncertainties. At the same time, carrier disturbance and complex nonlinearity should also be considered.

## III. CONTROLLER DESIGN

### A. ADRC ALOGRITHM

Number Airborne ISP system is affected by various factors such as working environment, nonlinear dynamics, and sensor noise. There are complex nonlinearities, strong external disturbances and uncertainties of model parameters in the ISP system. Therefore, the ADRC is designed to handle these complex factors that affect the control performance of the ISP system. Let $x_1 = \omega_p$, $x_2 = \dot{\omega}_p$, and consider external disturbance $d(t)$, then (1) can be rewritten as

$$\begin{aligned} \dot{x}_1 &= x_2 \\ \dot{x}_2 &= f(t, x, d) + bu \\ y &= x_1(t) \end{aligned} \tag{3}$$

where the total disturbance $f(t, x, d)$ is given by

$$f(t, x, d) = -\frac{f_d}{JT_i} x_1 - (\frac{1}{T_i} + \frac{f_d}{J}) x_2 + d \tag{4}$$

and $b = K_T / JT_i$.

Generating the TD is used to handle the contradictory between overshoot and quickness, and the second-order TD is

$$\begin{aligned} \dot{v}_1 &= v_2 \\ \dot{v}_2 &= \lambda^2 \psi(v_1 - r, \frac{v_2}{\lambda}) \end{aligned} \tag{5}$$

where $r$ is the reference input, $v_i\,(i = 1, 2)$ are the outputs, and $\lambda$ is the tunable speed coefficient. $\psi(v_1 - r, \frac{v_2}{\lambda})$ is a nonlinear function used to speed up convergence from $v_1$ to $r$.

ESO is the key of ADRC, and is usually used to estimate system states and total disturbance. Referring to equation (3), a third-order ESO is usually described as

$$\begin{aligned} \dot{z}_1 &= z_2 - \beta_1(z_1 - y) \\ \dot{z}_2 &= z_3 - \beta_2(z_1 - y) + bu \\ \dot{z}_3 &= -\beta_3(z_1 - y) \end{aligned} \tag{6}$$

where $z_i\,(i = 1, 2, 3)$ are the outputs of the ESO, $\beta_i > 0\,(i = 1, 2, 3)$ are the observer gains.

SEF is used to eliminate summation disturbances and perform state reconstruction, and the SEF is designed as:

$$\begin{cases} u = \dfrac{u_0 - z_3}{b} \\ u_0 = \sum\limits_{i=1}^{2} k_i (v_i - z_i) \end{cases} \tag{7}$$

where $k_i > 0\,(i = 1, 2)$ are the controller gains.

ADRC parameter tuning has always been an important topic due to it's a bunch of parameters. As suggested in [20], $\beta_i$ and $k_i$ are usually reduced to two tuning parameters for practical purposes: $\omega_c$, the controller bandwidth; and $\omega_o$, the observer bandwidth.

Defining the estimation errors

$$e_i = x_i - z_i (i = 1, 2, 3) \tag{8}$$

We get the error system:

$$\begin{aligned} \dot{e}_1 &= e_2 - \beta_1 e_1 \\ \dot{e}_2 &= e_3 - \beta_2 e_1 \\ \dot{e}_3 &= \dot{f} - \beta_3 e_1 \end{aligned} \tag{9}$$

Let $e = [e_1, e_2, e_3]^T$, (9) can be rewritten as follows:

$$e = Ae + B\dot{f} \tag{10}$$

where

$$A = \begin{bmatrix} -\beta_1 & 1 & 0 \\ -\beta_2 & 0 & 1 \\ -\beta_3 & 0 & 0 \end{bmatrix}, \quad B = \begin{bmatrix} 0 \\ 0 \\ 1 \end{bmatrix}$$

$\beta_i = \frac{(2+1)!}{i!(2-i+1)!}\omega_o^i$, $i = 1, 2, 3$. For $\omega_o > 0$, the state $e$ of (10) converges into a small field of origin, if there exist a positive constant $L$ that $\left|\dot{f}\right| \leq L$.

*Remark 1:* It follows Theorem 1 in [28] that the larger $\omega_o$, the higher the bandwidth of ESO, and the smaller the steady-state estimation errors. So $\omega_o$ is a tradeoff between performance and physical limitations. In addition, a large $\omega_c$ means fast response speed and strong anti-disturbance capability. However, the larger controller bandwidth and observer bandwidth also means the increase in the impact of sensor noise.

It can be seen from Fig.2 that the speed feedback of the stability loop is obtained by the differential of the position information measured by the encoder, so that a large noise is introduced. Low pass filters (LPF) may be an intuitive choice to attenuate sensor noise. However, as can be seen from Fig.3, simply adding LPF may make ADRC lose robustness. Suppose that the plant is given as

$$P(s) = \frac{0.8}{(0.001s + 1)(0.04s + 1)} \tag{11}$$

And $\omega_c = 500$, $\omega_o = 300$. The LPF is $Q(s) = \frac{1}{(\tau s+1)^2}$. The simulation results with 5% sensor noise are shown in Fig. 3, where it is seen that small $\tau$ can suppress the sensor noise, but when $\tau$ increases, the system overshoot will increase, and even the system will lose stability. However, when $\tau$ is small, the filtering effect of $Q(s)$ is often unsatisfactory. Therefore, ADRC with low-pass filter may not be able to achieve excellent control performance.

### B. NOISE REDUCTION DISTURBANCE OBSERVER

In this section, a modified DOB controller is developed from [25], [29] to eliminate the effect of sensor noise. The noise reduction disturbance observer (NR-DOB) proposed by [25] is shown in fig.4, and the system output $y$ and the control input $u$ are

$$\begin{aligned} y(s) &= T_{yr}(s)r(s) + T_{yd}(s)d(s) + T_{yn}(s)n(s) \\ u(s) &= T_{ur}(s)r(s) + T_{ud}(s)d(s) + T_{un}(s)n(s) \end{aligned} \tag{12}$$

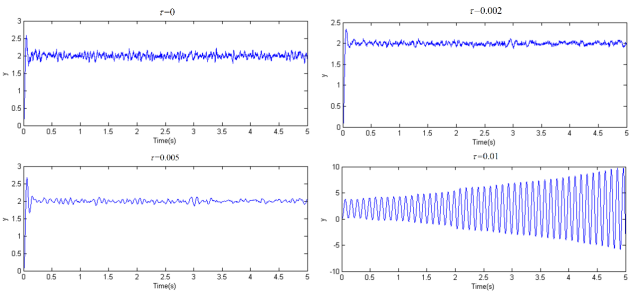


**FIGURE 3.** Simulation results for ADRC combined with LPF.

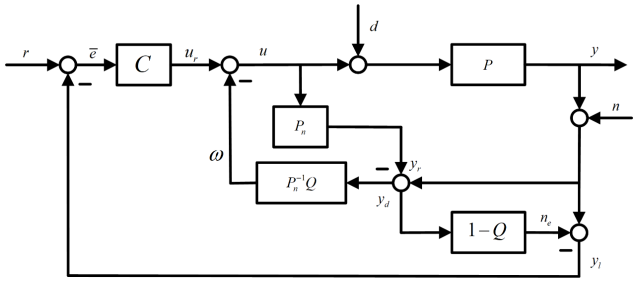


**FIGURE 4.** NR-DOB control system from [25].

where

$$\begin{aligned} T_{ur} &= \frac{P_n C}{(1 + P_n C)(P_n + Q(P - P_n))}, \quad T_{yr} = PT_{ur}, \\ T_{ud} &= \frac{-PQ}{P_n + Q(P - P_n)}, \quad T_{yd} = \frac{P_n P(1 - Q)}{P_n + Q(P - P_n)}, \\ T_{un} &= \frac{-Q}{P_n + Q(P - P_n)}, \quad Tyn = PT_{un}. \end{aligned}$$

where LPF $Q(s)$ is defined as

$$Q(s) = \frac{c_h(\tau s)^h + c_{h-1}(\tau s)^{h-1} + \cdots + c_0}{(\tau s)^l + a_{l-1}(\tau s)^{l-1} + \cdots + a_1(\tau s) + a_0} \tag{13}$$

where $\tau > 0$ is a constant, $h \geq 0$ and $l \geq 0$ are integers. Suppose that $c_0 = a_0, l \geq h+r : deg\,(P_n)$, and the numerator of $Q(s)$ is stable. Note that, the LPF $Q(s)$ satisfies

$$\begin{aligned} |Q(j\omega)| &\approx 1, \quad \omega \in [0, \omega_L] \\ |Q(j\omega)| &\approx 0, \quad \omega \in [\omega_H, \infty] \end{aligned} \tag{14}$$

when $\omega \in [0, \omega_L]$, from (12) we have

$$T_{yr}(j\omega) \approx \frac{P_n C}{1 + P_n C}\Big|_{s=j\omega} \tag{15}$$

$$T_{yd}(j\omega) \approx P_n(1 - Q)\Big|_{s=j\omega} \approx 0 \tag{16}$$

When $\omega \in [\omega_H, \infty]$, $T_{yn}(j\omega) \approx -\frac{PQ}{P_n}(j\omega) \approx 0$, $T_{un}(j\omega) \approx \frac{-Q}{P_n}(j\omega) \approx 0$. Therefore, by selecting the appropriate $Q(s)$, Sensor noise can be filtered out by NR-DOB in [25].

Although the NR-DOB designed in [25] can effectively deal with model uncertainty, an accurate $P_n$ is still expected for better control performance. However, a complex $P_n$ will consume a lot of hardware resources. And for the ISP stability loop, a high calculation frequency is required. Therefore, when designing NR-DOB, $P_n$ should be used as little as

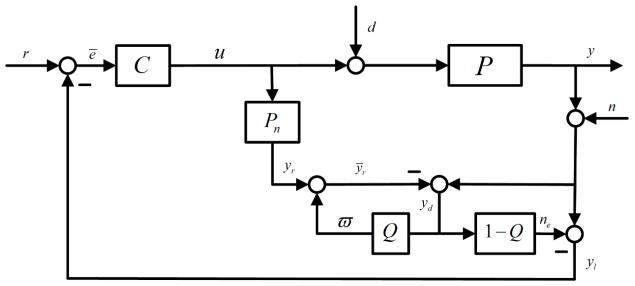


**FIGURE 5.** A simplified noise reduction disturbance observer.

possible to simplify the control algorithm. On the other hand, it follows (12) that the disturbance attenuation capability of NR-DOB is only related to NR-DOB, but not to the outer loop controller. The combination of NR-DOB and ADRC will offset the superiority of ADRC. a simplified NR-DOB (SNR-DOB) shown in Fig.5 is proposed, from which we can see that $P_n^{-1}$ is eliminated. The system output $y$ and control input $u$ are calculated as the same form (12), and

$$\begin{aligned} T_{ur} &= \frac{(1+Q)C}{(1-Q)P_nC+1+Q+2PCQ}, \quad T_{yr} = PT_{ur}, \\ T_{ud} &= \frac{-2PCQ}{(1-Q)P_nC+1+Q+2PCQ}, \\ T_{yd} &= \frac{P((1-Q)P_nC+1+Q)}{(1-Q)P_nC+1+Q+2PCQ}, \\ T_{un} &= \frac{-2CQ}{(1-Q)P_nC+1+Q+2PCQ}, \quad Tyn = PT_{un}. \end{aligned} \tag{17}$$

In $[0, \omega_L]$, it follows from (17) that

$$T_{yr}(j\omega) \approx \frac{PC}{1+PC}\Big|_{s=j\omega} \tag{18}$$

Therefore, even $\omega \in [0, \omega_L]$, the tracking performance of SNR-DOB is quite different from that of NR-DOB and DOB, but it is also approximated to the nominal one. And

$$T_{yd}(j\omega) \approx \frac{P}{1+PC}\Big|_{s=j\omega} \tag{19}$$

(19) has the same perturbation attenuation characteristics as the system controlled only by $C(s)$. Therefore, the SNR-DOB itself has almost no anti-disturbance capability while the NR-DOB of [25] has this ability. Instead, the role of $\varpi$ in Fig.5 is to ensure that $y_l$ retains as much disturbance information as possible so that controller $C(s)$ can achieve perturbation attenuation.

In the high frequency range $\omega \in [\omega_H, \infty]$,

$$\begin{aligned} T_{yn}(j\omega) &\approx -\frac{2PCQ}{1+P_nC}\Big|_{s=j\omega} \approx 0 \\ T_{un}(j\omega) &\approx -\frac{2CQ}{1+P_nC}\Big|_{s=j\omega} \approx 0 \end{aligned} \tag{20}$$

Therefore, like NR-DOB in Figure 4, SNR-DOB can also suppress sensor noise by selecting the appropriate $Q(s)$ whereas DOB controller cannot eliminate the effect of sensor noise.

*Remark 2:* Since (14) is a very rough approximation, (16) and (19) cannot indicate that the anti- disturbance ability of the system in Fig.4 is stronger than that of in Fig. 5. In addition, (12) shows that the disturbance attenuation capability of the NR-DOB system is only related to the inner loop, and is independent of the outer loop controller $C(s)$. Therefore, optimizing its outer loop controller does not improve the system's anti-disturbance capability. The SNR-DOB system's anti-disturbance capability is directly related to $C(s)$, so it can be combined with many advanced control methods for better control performance.

## IV. ROBUST STABILITY

This section focuses on the robust stability of SNR-DOB system. For this purpose, the following systems with parameter uncertainties are considered.

*Assumption 1:* Let the set $\wp$ of transfer functions be

$$\wp = \left\{ P(s) = \frac{\gamma_{n-r}s^{n-r} + \gamma_{n-r-1}s^{r-n-1} + \cdots + \gamma_0}{\alpha_n s^n + \alpha_{n-1}s^{n-1} + \cdots + \alpha_0} : \begin{matrix} \\ \alpha_i \in [\alpha_i, \overline{\alpha}_i],\ \gamma_i \in [\gamma_i, \overline{\gamma}_i] \end{matrix} \right\} \tag{21}$$

where $n$ and $r$ are positive integers, and all $\alpha_i$, $\overline{\alpha}_i$, $\gamma_i$ and $\overline{\gamma}_i$ are known constants such that $0 \notin [\alpha_i, \overline{\alpha}_i]$ and $0 \notin [\gamma_i, \overline{\gamma}_i]$. Suppose that both $P(s)$ and $P_n(s)$ are belongs to $\wp$. $P_n(s)$ is chosen such that $P(s)$ and $P_n(s)$ have the same relative order.

With the configuration of Fig. 5, twelve transfer functions from $[r, d, n]^T$ to $[u, y, y_r, \overline{e}]^T$ are given by

$$\frac{1}{\Delta(s)}\begin{bmatrix} (1+Q)C & -2PCQ & -2QC \\ (1+Q)PC & (1-Q)P_nC+1+Q & -2PQC \\ (1+Q)P_nC & -2PP_nCQ & -2P_nQC \\ (1+Q) & -2PQ & -2Q \end{bmatrix} \tag{22}$$

where $\Delta(s) = (1-Q)P_nC+1+Q+2PCQ$. If the above twelve transfer functions are stable, then the closed loop system is said to be internally stable. Write $P$, $P_n$, $C$, $Q$ as ratios of coprime polynomials; that is $P(s) = \frac{N(s)}{D(s)}$, $P_n(s) = \frac{N_n(s)}{D_n(s)}$, $C(s) = \frac{N_C(s)}{D_C(s)}$, and $Q(s) = \frac{N_Q(s)}{D_Q(s)}$. Then, (22) is rewritten as

$$\frac{1}{\delta(s,\tau)}\begin{bmatrix} M_{11} & M_{12} & M_{13} \\ M_{21} & M_{22} & M_{23} \\ M_{31} & M_{32} & M_{33} \\ M_{41} & M_{42} & M_{43} \end{bmatrix} \tag{23}$$

where $\delta(s;\tau) := DN_nN_C(D_Q - N_Q) + D_QD_CD_nD + N_QD_CD_nD + 2D_nNN_CN_Q$, and $M_{ij}$ are calculated by (22). Thus, the SNR-DOB control system is internally stable if and only if all the eigenvalues of $\delta(s;\tau)$ in (23) are located in the left half plane for $P(s) \in \wp$. Let $m := deg\,(D_CD_nD)$. Since all the transfer functions $P$, $P_n$, $C$, and $Q$ are proper, $deg\,(\delta(s;\tau)) = m+l$ with $\tau > 0$, i.e. there exists $m+l$ roots of the equation $\delta(s;\tau) = 0$.

*Lemma 1:* Let

$$\begin{aligned} P_s(s) &:= 2D_n(DD_C + NN_C) \\ P_f(s) &:= D_Q(s;1) + N_Q(s;1) \end{aligned} \tag{24}$$

The polynomials $P_s(s)$ and have $P_f(s)m$, and $l$ roots, respectively. Let $s_1^* \cdots s_m^*$ and $s_{m+1}^* \cdots s_{m+l}^*$ be the roots of $P_s(s) = 0$ and $P_f(s) = 0$, respectively. Then, the following conditions hold.

$$\begin{aligned} \lim_{s\to\infty} s_i(\tau) &= s_i^*, i = 1, \ldots, m \\ \lim_{s\to\infty} \tau s_i(\tau) &= s_i^*, i = m+1, \ldots, m+l \end{aligned} \tag{25}$$

where $s_i^* (i = 1, \ldots, m + l)$ are the roots of $\delta(s; \tau) = 0$.

*Proof:* Since $D_Q(s; 0) = N_Q(s; 0) = a_0 = 0$, it follows that $\delta(s; 0) = 2a_0 D_n(D_C D + NN_C) = a_0 P_s(s)$. Thus, m roots of $\delta(s; \tau) = 0$ converge to those of $P_s(s) = 0$ as $\tau$ approaches zero. To investigate the remaining $l$ roots of $\delta(s; \tau) = 0$, let

$$\begin{aligned} \overline{\delta}(s; \tau) &:= \tau^m \delta(\frac{s}{\tau}; \tau) \\ &= \eta_1(s; \tau) D_Q(\frac{s}{\tau}; \tau) + \eta_2(s; \tau) N_Q(\frac{s}{\tau}; \tau) \end{aligned} \tag{26}$$

where $\eta_1(s; \tau) = \tau^m(DN_nN_C(s/\tau) + D_C D_n D(s/\tau))$ and $\eta_2(s; \tau) = \tau^m(DN_nN_C(s/\tau) + D_C D_n D(s/\tau) + 2D_nNN_C(s/\tau))$. Since $P$, $P_n$, $C$, and $Q$ are proper, it follows that $\lim_{\tau\to 0} \eta_1(s; \tau) = \lim_{\tau\to 0} \tau^m D_C D_n D(s/\tau) = \overline{\eta}_1 s^m$ and $\lim_{\tau\to 0} \eta_2(s; \tau) = \lim_{\tau\to 0} \tau^m D_C D_n D(s/\tau) = \overline{\eta}_1 s^m = \overline{\eta}_1 s^m$ for all $s$ with some constants $\overline{\eta}_1$. On the other hand, because $D_Q(s/\tau; \tau) = D_Q(s; 1)$ and $N_Q(s/\tau; \tau) = N_Q(s; 1)$, we obtain $\overline{\delta}(s; 0) = \overline{\eta}_1 s^m[D_Q(s; 1) + N_Q(s; 1)] = \overline{\eta}_1 s^m P_f(s)$. Therefore, there exist $m$ roots of $\overline{\delta}(s; \tau) = 0$ at the origin and $l$ roots at $s_{m+1}^* \cdots s_{m+l}^*$. Therefore, it fellows from **Lemma 1** of [30], there are $l$ roots of $\overline{\delta}(s; \tau) = 0$, say $\overline{s}_i (i = 1, \ldots, m + l)$, such that $\lim_{\tau\to 0} \overline{s}_i(\tau) = s_i^*$, i.e. $\overline{s}_i(\tau)/\tau$ are the roots of $\delta(s; \tau) = 0$. Hence (25) is proved.

According to **Lemma 1**, an almost sufficient and necessary condition for the robustly internal stability of the SNR-DOB control system are presented.

*Theorem 1:* Under **Assumption 1**, for all $\tau > 0$, and $0 < \tau \leq \tau^*$, the SNR-DOB control system is said to be robustly internally stable if the following three conditions hold

(a) $P_n(s)$ is stable,

(b) $PC/(l + PC)$ is stable for all $P(s) \in \wp$, and

(c) $P_f(s)$ is Hurwitz.

*Proof:* The denominators of $PC/(l + PC)$ and $P_n(s)$ are $DD_C + NN_C$ and $D_n(s)$, respectively. Thus, (a) and (b) means that $P_s(s)$ is Hurwitz. Therefore, the proof fellows **Lemma 1**.

*Remark 3:* An important condition for robust internal stability of NR-DOB system of [25] is that $P(s)$ is the minimum phase system. which is not required by the proposed SNR-DOB system. The condition (b) is a basic requirement for feedback control systems. Even if $P(s)$ is unstable and non-minimum phase, the SNR-DOB system can also be robustly stabilized by the appropriate controller $C(s)$, and the ADRC can usually meet this requirement [9]. And whether the $P_f(s)$ of NR-DOB system is Hurwitz is related to the selected $P(s)$, $P_n(s)$ and $Q(s)$, while the $P_f(s)$ of SNR-DOB system is only related to $Q(s)$. In addition, the SNR-DOB system in Fig.5 is much simpler because $P_n^{-1}(s)$ is eliminated. At the same time, as can be seen from Fig.4 that for NR-DOB system $r : deg(Q) \geq r : deg(P_n)$ is required to satisfy the regularity, while this condition is not required by SNR-DOB system. Thus, the relative order of the Q-filter can be arbitrary in the SNR-DOB system, and it is clear that lower order Q-filters make the control algorithm simpler.

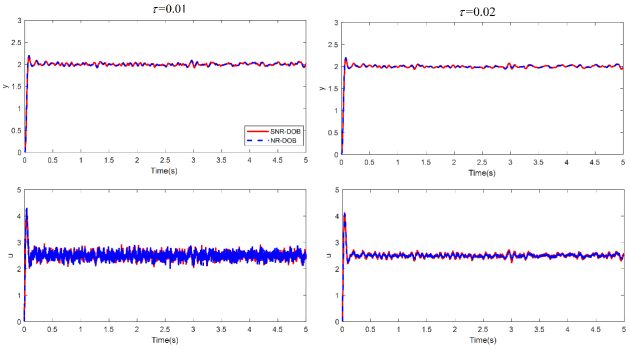


**FIGURE 6.** Simulation results of the step response by the two control methods.

*Remark 4:* The control object becomes $PQ$ instead of $P(s)$ when ADRC and LPF are simply combined. Correspondingly, $Q(s)$ is introduced into the ADRC control system as a modeling error. Thus, the robustness of ADRC is deteriorated. In contrast, the robust stability of SNR-DOB depends mainly on condition (b) of **Theorem 1** for the other two conditions are easily satisfied. Condition (b) is the same as the closed-loop system transfer function without the LPF. Therefore, for ADRC, the SNR-DOB controller is more robust than simply adding LPF.

## V. SIMULATIONS AND EXPERIMENTS

### A. SIMULATIONS

Note that the anti-disturbance ability of NR-DOB system is independent of outer-loop controller $C(s)$. When $P_n(s) \neq P(s)$, the system may not be able to track accurately because of the total disturbance feedback of outer-loop ADRC (This conclusion was obtained by simulation, but without rigorous theoretical proof). In order to compare SNR-DOB with NR-DOB, and to show that these two methods are superior to LPF, consider plant (11) and let $P_n(s) = P(s)$. The Q-filter is simply chosen as

$$Q(s) = \frac{1}{(\tau s + 1)^2} \tag{27}$$

Obviously, $P_n(s)$ is stable and for all $\tau > 0 P_f(s)$ is Hurwitz. Let $\omega_c = 500$, $\omega_o = 300$, then it is easy to know from Fig. 3 that $PC/(l + PC)$ is also stable.

The simulation results with 5% sensor noise are shown in Fig.6, in which the noise levels of the two control methods are almost the same. It can be seen that compared with Fig.3, the overshoot of the two control methods is significantly reduced in the case of effective filtering of noise. And as $\tau$ increases, the noise filtering effect increases while the overshoot remains unchanged. Sinusoidal input disturbances were added to compare the anti-disturbance capabilities of the two

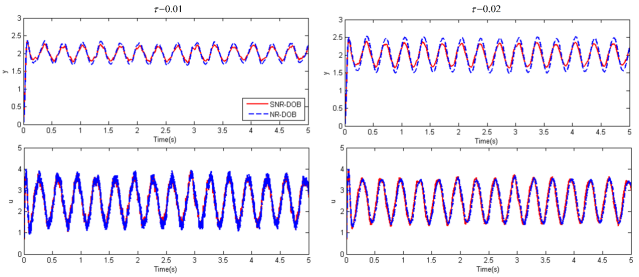


**FIGURE 7.** Simulation results with input disturbance by the two control methods.

control methods. Fig.7 shows the simulation results. It can be seen that the SNR-DOB has superior anti-disturbance ability than NR-DOB under the same outer loop controller.

### B. EXPERIMENTS

To verify the practicability and effect of the proposed algorithm, the experiments are completed. The control objective is to adjust the stability loop of the ISP with input disturbance and sensor noise for greater anti-disturbance and rapidity. Since the two axes of the two-axis ISP are similar, the laboratory experiment only shows the experimental results of the yaw gimbal with greater inertia and friction. The control algorithm is implemented by DSPTMS320F28335, and the sampling frequency is 1kHz. $P_n(s)$ is selected as

$$P_n(s) = \frac{8}{(0.00067s+1)(0.02s+1)} \tag{28}$$

$Q(s)$ is the same as in (27) and $\tau = 0.01$. The outer loop controller $C_1(s)$ of SNR-DOB is a ADRC controller with $\omega_c = 500$, $\omega_o = 200$, and the outer loop controller $C_2(s)$ of NR-DOB is simply chosen as a PI controller (When $P_n(s) \neq P(s)$, the system may not be able to track accurately because of the total disturbance feedback of outer-loop ADRC).

$$C_2 = 0.04 + 0.03\frac{1}{s} \tag{29}$$

The experimental results of the step response are shown in Fig. 8, where the speed reference is set to $2°/s$. from which we can see that the noise in the output and control inputs of SNR-DOB and NR-DOB is approximately at the same level. However, due to different outer loop controllers, SNR-DOB has almost no overshoot while NR-DOB has obvious overshoot. Two sinusoidal input disturbances $\sin(2\pi t)$ and $0.2\sin(10\pi t)$ were added to compare the anti-disturbance capabilities of the two methods, and the experimental results are shown in Fig.9. It can be seen that the anti-disturbance capability of SNR-DOB is about 1/3 higher than that of NR-DOB. The sinusoidal response experiments with two different frequency references $\sin(4\pi t)$ and $\sin(10\pi t)$ were conducted in Fig.10 to compare the tracking accuracy of the two methods. For SNR-DOB, the RMS (root mean square) of the tracking deviations are $0.146°/s$ and $0.176°/s$, respectively; for NR-DOB, the RMS are $0.247°/s$ and $0.297°/s$, respectively.

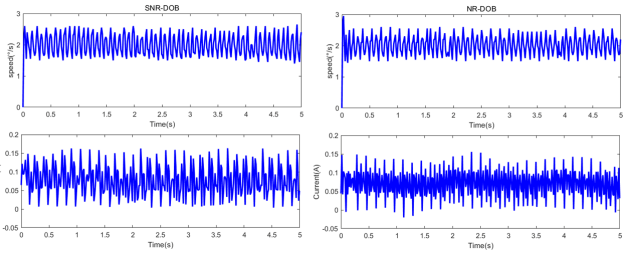


**FIGURE 8.** Experimental results of the step response by the two control methods.

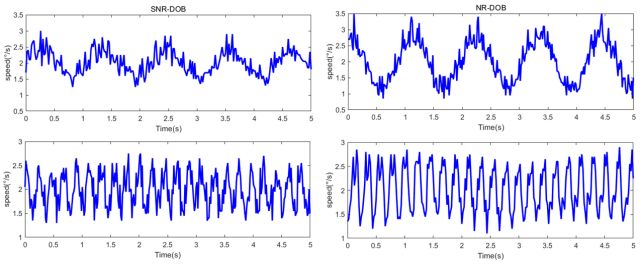


**FIGURE 9.** Experimental results with input disturbances by the two control methods.

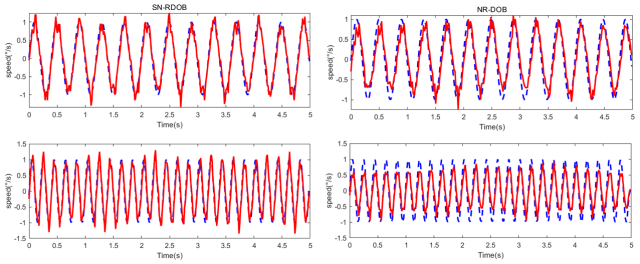


**FIGURE 10.** Experimental results of the sinusoidal response by the two control methods.

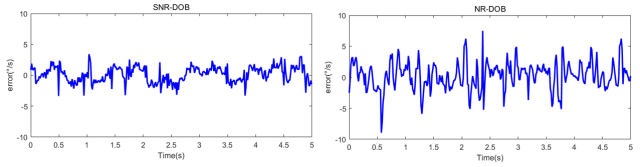


**FIGURE 11.** Experimental results in a vibrating environment by the two control methods.

Overall, the tracking deviation of the former method is about 60% of the latter.

ISP experiments in a vibrating environment were implemented to compare the combined effects of tracking performance and anti-disturbance capabilities of the two methods, and the experimental results are shown in Fig.11. Fig.11 shows the deviations between the yaw gimbal speed of the ISP and the gyroscope output. The RMS are $1.008°/s$ for SNR-DOB and $2.260°/s$ NR-DOB.

In order to more effectively verify the effect of the proposed algorithm, the vehicle tracking star experiments were carried out in the Huan Cheng Expressway in Xi'an,


**FIGURE 12.** Vehicle experiment system.

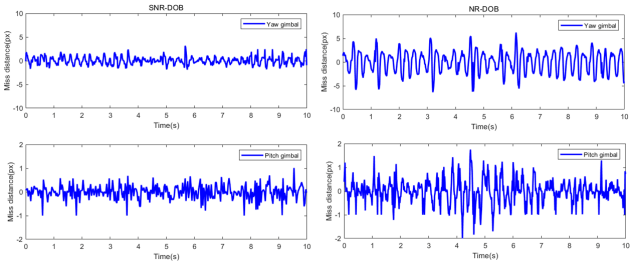


**FIGURE 13.** Comparison of vehicle experiment results: Static situation.

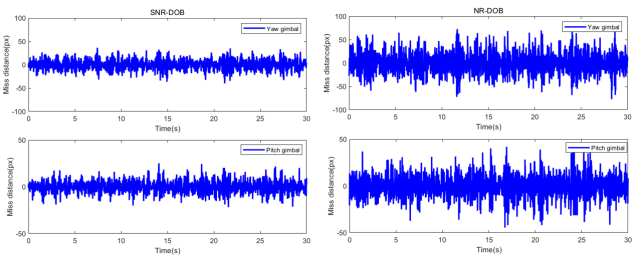


**FIGURE 14.** Comparison of vehicle experiment results: Motion situation.

Shaanxi Province. The vehicle and the star tracker ISP are shown in Fig.12. The star tracker ISP system was mounted on the top of the vehicle. During the experiment, the vehicle traveled at a constant speed of 80km/h, and the star tracker ISP captured and continuously tracked the target star.

The output miss distances of camera were used as criteria of the control system. The miss distances of two gimbals, when the vehicle is stationary, are shown in Fig.13. The experimental results of two different methods are as follows: for SNR-DOB: the yaw gimbal's RMS is 0.800px that is 34.82% of NR-DOB and pitch gimbal's RMS is 0.23px that is 46.37% of NR-DOB. The experimental results of tracking the same star under vehicle motion are shown in Fig.14. For SNR-DOB: the yaw gimbal's RMS is 10.962px that is 49.92% of NR-DOB and pitch gimbal's RMS is 6.303px that is 55.56% of NR-DOB.

## VI. CONCLUSION

In this paper, a control strategy based on active disturbance rejection control (ADRC) with a simple noise reduction disturbance observer (SNR-DOB) is proposed to improve the line of sight (LOS) stabilization accuracy of the two-axis inertial stabilization platform (ISP) for airborne star tracker application. ADRC is used to estimate and compensate the system nonlinearities, parameter uncertainties, and disturbances. And SNR-DOB is proposed to achieve noise suppression and improve anti-disturbance capability and rapidity of the system. NR-DOB was first developed in [25], It can be seen that SNR-DOB has a simpler structure, and its anti-disturbance capability can be optimized by the outer loop controller while NR-DOB cannot. The contrast experiments show that the proposed method has stronger anti-disturbance ability and rapidity than the method in [25]. The vehicle tracking star experiment results show that the proposed method can achieve high-precision LOS stability.

## REFERENCES

[1] X. Zhou, B. Zhao, W. Liu, H. Yue, R. Yu, and Y. Zhao, "A compound scheme on parameters identification and adaptive compensation of nonlinear friction disturbance for the aerial inertially stabilized platform," *ISA Trans.*, vol. 67, pp. 293–305, Mar. 2017.

[2] Y. Han, Y. Lu, and H. Qiu, "An improved control scheme of gyro stabilization electro-optical platform," in *Proc. IEEE Int. Conf. Control Automat.*, Guangzhou, China, May/Jun. 2007, pp. 346–351.

[3] F. Dong, X. Lei, and W. Chou, "A dynamic model and control method for a two-axis inertially stabilized platform," *IEEE Trans. Ind. Electron.*, vol. 64, no. 1, pp. 432–439, Jan. 2017.

[4] X. Zhou, H. Zhang, and R. Yu, "Decoupling control for two-axis inertially stabilized platform based on an inverse system and internal model control," *Mechatronics*, vol. 24, no. 8, pp. 1203–1213, Dec. 2014.

[5] J. Fang, R. Yin, and X. Lei, "An adaptive decoupling control for three-axis gyro stabilized platform based on neural networks," *Mechatronics*, vol. 27, pp. 38–46, Apr. 2015.

[6] Q. Mu, G. Liu, and X. Lei, "A RBFNN-based adaptive disturbance compensation approach applied to magnetic suspension inertially stabilized platform," *Math. Problems Eng.*, vol. 2014, Aug. 2014, Art. no. 657985.

[7] J. Mao, J. Yang, S. Li, and Q. Li, "Output feedback stabilization of inertial stabilized platform with unmatched disturbances using sliding mode approach," *IFAC-PapersOnLine*, vol. 50, no. 1, 5149-5154, Jul. 2017.

[8] S. Liu, H. Che, and L. Sun, "Research on stabilizing and tracking control system of tracking and sighting pod," *J. Control Theory Appl.*, vol. 10, no. 1, pp. 107–112, Feb. 2012.

[9] W. Tan and C. Fu, "Linear active disturbance-rejection control: Analysis and tuning via IMC," *IEEE Trans. Ind. Electron.*, vol. 63, no. 4, pp. 2350–2359, Apr. 2016.

[10] A. Rubaai and P. Young, "Hardware/software implementation of fuzzy-neural-network self-learning control methods for brushless DC motor drives," *IEEE Trans. Ind. Appl.*, vol. 52, no. 1, pp. 414–424, Jan./Feb. 2015.

[11] Y. Zhang, T. Yang, C. Li, S. Liu, C. Du, M. Li, and H. Sun, "Fuzzy-PID control for the position loop of aerial inertially stabilized platform," *Aerosp. Sci. Technol.*, vol. 36, pp. 21–26, Jul. 2014.

[12] P. Song, "Robust control of gyro stabilized platform driven by ultrasonic motor," *Sens. Actuators A, Phys.*, vol. 261, pp. 280–287, Jul. 2017.

[13] L. H. Keel and S. P. Bhattacharyya, "Robust, fragile, or optimal?" *IEEE Trans. Autom. Control*, vol. 42, no. 8, pp. 1098–1105, Aug. 1997.

[14] M. S. Sofla, M. Zareinejad, M. Parsa, and H. Sheibani, "Integral based sliding mode stabilizing a camera platform using Kalman filter attitude estimation," *Mechatronics*, vol. 44, pp. 42–51, Jun. 2017.

[15] X. Zhou, Y. Li, Y. Jia, and L. Zhao, "An improved fuzzy neural network compound control scheme for inertially stabilized platform for aerial remote sensing applications," *Int. J. Aerosp. Eng.*, vol. 2018, Aug. 2018, Art. no. 7021038.

[16] X. Zhang, Y. Zhao, K. Guo, G. Li, and N. Deng, "An adaptive b-spline neural network and its application in terminal sliding mode control for a mobile satcom antenna inertially stabilized platform," *Sensors*, vol. 17, no. 5, p. 978, Apr. 2017.

[17] F. Liu, H. Wang, Q. Shi, H. Wang, M. Zhang, and H. Zhao, "Comparison of an ANFIS and fuzzy PID control model for performance in a two-axis inertial stabilized platform," *IEEE Access*, vol. 5, pp. 12951–12962, 2017.
[18] J. Q. Han, "Auto disturbance rejection controller and it's applications," (in Chinese), *Control Decis.*, vol. 13, no. 1, pp. 19–23, 1998.
[19] J. Han, "From PID to active disturbance rejection control," *IEEE Trans. Ind. Electron.*, vol. 56, no. 3, pp. 900–906, Mar. 2009.
[20] Z. Gao, "Scaling and bandwidth-parameterization based controller tuning," in *Proc. Amer. Control Conf.*, Denver, CO, USA, Jun. 2003, pp. 4989–4996.
[21] W. Xue and Y. Huang, "On performance analysis of ADRC for a class of MIMO lower-triangular nonlinear uncertain systems," *ISA Trans.*, vol. 53, no. 4, pp. 955–962, Jul. 2014.
[22] B. Ahi and A. Nobakhti, "Hardware implementation of an ADRC controller on a gimbal mechanism," *IEEE Trans. Control Syst. Technol.*, vol. 26, no. 6, pp. 2268–2275, Nov. 2018.
[23] X. Zhou, H. Gao, B. Zhao, and L. Zhao, "A GA-based parameters tuning method for an ADRC controller of ISP for aerial remote sensing applications," *ISA Trans.*, vol. 81, pp. 318–328, Oct. 2018.
[24] A. Safa and R. Y. Abdolmalaki, "Robust output feedback tracking control for inertially stabilized platforms with matched and unmatched uncertainties," *IEEE Trans. Control Syst. Technol.*, vol. 27, no. 1, pp. 118–131, Jan. 2019.
[25] N. H. Jo, C. Jeon, and H. Shim, "Noise reduction disturbance observer for disturbance attenuation and noise suppression," *IEEE Trans. Ind. Electron.*, vol. 64, no. 2, pp. 1381–1391, Feb. 2017.
[26] S. Cheong, S. H. Oh, and S.-Y. Lee, "Support vector machines with binary tree architecture for multi-class classification," *Neural Inf. Process., Lett. Rev.*, vol. 2, no. 3, pp. 47–51, Mar. 2004.
[27] X. Song, H. Chen, and Y. Xue, "Stabilization precision control methods of photoelectric aim-stabilized system," *Opt. Commun.*, vol. 351, no. 15, pp. 115–120, Sep. 2015.
[28] F. Alonge, M. Cirrincione, F. D'Ippolito, M. Pucci, and A. Sferlazza, "Robust active disturbance rejection control of induction motor systems based on additional sliding-mode component," *IEEE Trans. Ind. Electron.*, vol. 64, no. 7, pp. 5608–5621, Jul. 2017.
[29] W. Xie, "High frequency measurement noise rejection based on disturbance observer," *J. Franklin Inst.*, vol. 347, no. 10, pp. 1825–1836, Dec. 2010.
[30] H. Shim and N. H. Jo, "An almost necessary and sufficient condition for robust stability of closed-loop systems with disturbance observer," *Automatica*, vol. 45, no. 1, pp. 296–299, Jan. 2009.

**FAN WANG** received the bachelor's degree in mechanical and electrical engineering from the School of Engineering and Mechanical Engineering, Chang'an University, China. He is currently pursuing the Ph.D. degree with the Institute of Optics and Electronics, Chinese Academy of Sciences. His research interests include active disturbance rejection control and nonlinear control theory.

**RANJUN WANG** received the Ph.D. degree from the Institute of Optics and Electronics, Chinese Academy of Sciences, Chengdu, China, in 2012, where he is currently an Associate Professor. His research interests include aerospace electrical design, embedded software development, and disturbance rejection control theory.

**ENHAI LIU** is currently a Researcher and a Ph.D. Tutor. He is currently the Deputy Director of the Institute of Optics and Electronics, Chinese Academy of Sciences. His research interests include space optoelectronic precision measurement, photodetector application and photodetection technology, signal and information processing, optoelectronic measurement system error theory analysis, system integration technology research, and undertaken and completed a number of manned spaceflight and lunar exploration in related fields. The research (development) of the engineering, 863 and 973 engineering projects received four awards for provincial and ministerial level scientific and technological progress. He is a member of the Chinese Optical Society, the Optical Engineering Society, and the Space Optical Engineering Society. He is a member of the Academic and Academic Degree Committee and is engaged in research and engineering research on photoelectric precision measurement and automatic control technology.

**WENMING ZHANG** received the master's degree from the University of Electronic Science and Technology, China, in 2004. He is currently an Associate Professor with the Institute of Optics and Electronics, Chinese Academy of Sciences. He is mainly engaged in the research and development of various military or civil optical measurement system technologies and precision optical instruments. He has accumulated more than 20 years of experience in optical measurement systems, optical instruments, and satellite ground-based simulation test equipment. He is working on the development and research of ground optical simulation test equipment for optical target detection and control systems for a variety of space target aircraft. His current research interests include optical simulation and optical engineering measurement techniques.